Synsint Research Group

Available online at www.synsint.com

Synthesis and Sintering

**ISSN** 2564-0186 (Print), **ISSN** 2564-0194 (Online)

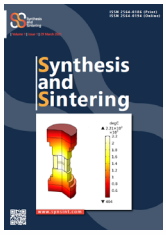


*Research article*

# In-situ synthesis of TiN and $TiB_2$ compounds during reactive spark plasma sintering of BN–Ti composites

**Maryam Abdolahpour Salari** [a,*], **Günay Merhan Muğlu** [b], **Mohsen Rezaei** [c], **M. Saravana Kumar** [d], **Harikrishnan Pulikkalparambil** [e], **Suchart Siengchin** [e]

[a] *Department of Physics, Faculty of Sciences, Ataturk University, Erzurum, Turkey*
[b] *Hınıs Vocational College, Department of Medical Services and Techniques, Ataturk University, Erzurum, Turkey*
[c] *Department of Chemistry, Faculty of Sciences, Ataturk University, Erzurum, Turkey*
[d] *Department of Mechanical Engineering, Mount Zion College of Engineering and Technology, Pudukkottai, Tamil Nadu, India*
[e] *Department of Materials and Production Engineering, The Sirindhorn International Thai-German Graduate School of Engineering (TGGS), King Mongkut's University of Technology North Bangkok, Bangkok, 10800, Thailand*

A B S T R A C T

A BN–$TiB_2$–TiN composite was produced via reactive sintering of the hexagonal BN (hBN) with 20 wt% Ti. Spark plasma sintering (SPS) was used as the fabrication method and the sample was characterized by X-ray diffractometry, energy-dispersive X-ray spectroscopy, and scanning electron microscopy. According to the results, the Ti was utterly consumed during the SPS, led to the in-situ $TiB_2$ and $TiN_{0.9}$ formations. Additionally, the microstructural study revealed the nucleation and growth of new hBN platelets from the initial fine hBN particles. Anyway, the final composite reached a relative density of 95%, because of the remaining free spaces between the hBN platelets. It was found that some nitrogen and boron atoms could leave the TiN and $TiB_2$ microstructures, respectively, and diffuse into the opposing phase.


K E Y W O R D S

Boron nitride
Titanium
Reactive spark plasma sintering
In-situ phases
Synthesis

OPEN ACCESS

## 1. Introduction

Hexagonal boron nitride is an advanced ceramic with a crystalline structure similar to graphite, namely a lamellar one [1–4]. This material owns a unique combination of features, e.g., low elastic modulus, low density, high thermal conductivity, good thermal shock resistivity, high refractoriness, high abrasion resistivity, excellent corrosion resistivity, and significant dielectric and insulation characteristics, as well as good machinability, which makes it a suitable nominee for an extended range of industrial applications, such as thermocouples' insulating sleeves, crucibles, protection tubes, and high-temperature furnaces [5–11]. Additionally, this material possesses poor overall hardness owing to having the weak inter-layer van der Waals bonding [12]. Nevertheless, having both anisotropic lamellar structure as well as powerful covalent bonding has made the sintering process of this material challenging [13, 14]. Although grain coarsening is highly prohibited due to the low diffusion coefficient of hBN, the lamellar structure of this substance results in remaining porosity between the plates [4]. To overcome the mentioned difficulties, the implementation of advanced sintering techniques and also the incorporation of sintering additives can be the solution.

The pressureless sintering (PS) [15–18], hot-pressing (HP) [19–23], and sintering by spark plasma (SPS) [24–29] are amongst the most used processes for sintering of ceramic materials. The first route, i.e., pressureless sintering, is considered as a commercial technique, while the utilization of two others can lead to fabricating high-quality compounds thanks to their intrinsic characteristics, namely

* Corresponding author. *E-mail address:* m.salari@atauni.edu.tr (M. Abdolahpour Salari)
Received 13 March 2021; Received in revised form 16 April 2021; Accepted 20 April 2021.

https://doi.org/10.53063/synsint.2021.119

simultaneous external pressure and comparably low sintering temperature [1, 30–33]. Moreover, many scientists performed numerous researches works to improve both qualifications and sinterability of hBN via introducing an appropriate sintering additive, including Ti, Ni, TiN, $CaB_2O_4$, MAS, YAG, $SiO_2$, MgO, CaO, $B_2O_3$, $Al_2O_3$, $Y_2O_3$, and so forth [4, 12, 30, 31, 34–38].

Kitiwan et al. [38] studied the densification behavior as well as phase transformation of the SPSed hBN–TiN composites produced at four different sintering temperatures, i.e., 1700, 1800, 1900 and 2000 °C. According to their results, the relative density of samples was linearly increased with rising TiN amount from 10 to 90 vol%. As a result, the highest percentage of relative density (almost 97%) was secured for the sample containing 90% TiN SPSed at 2000 °C. Also, the formation of $TiB_2$ as an in-situ phase was reported at all sintering temperatures, excluding the lowest one, namely 1700 °C. They also investigated the TiN–$TiB_2$–hBN composites fabricated by the SPS route at 1700 °C under 100 MPa for 5 min. In this research, the composites were containing between 0 to 30 vol% BN, while the ratio of $TiB_2$/TiN was maintained aound 70:30 (vol%). All samples reached the relative density values in the range of 96–97%; however, the optimum mechanical qualifications were attained at hBN content of 15%. Finally, Olevsky et al. [35] scrutinized the hBN/Ti composites produced via the pressureless sintering route. In terms of the hBN/Ti system with an atomic percent ratio of 2:3, the results endorsed the full consumption of the raw materials and the in-situ synthesis of $TiB_2$ and TiN compounds (at sintering temperate of 1200 °C for 20 hours).

In this research paper, we have tried to assess the impact of incorporating 20 wt% Ti as an additive on the microstructure of hBN. For this aim, the spark plasma sintering method at 1900 °C was engaged to densify the composite specimen. Additionally, energy-dispersive X-ray spectroscopy, scanning electron microscopy, and X-ray diffractometry were employed to investigate the SPSed sample.

## 2. Experimental procedure

In this investigation, commercially accessible powders of titanium and boron nitrides were used as the initial materials. A brief of the characteristics of such substances is exhibited in Table 1. First of all, the needed amount of each powder was weighed to fabricate BN-based samples containing 20 wt% Ti as an additive. Subsequently, the powder mixture was ultrasonically dispersed for 40 min in ethanol. In order to remove the already added ethanol as well as applying more efficient mixing, the resulted slurry was heated for two hours at 125 °C using a hot-plate shaker. After that, complete dehumidification was carried out for 24 hours at 100 °C using a universal oven. A uniform powder mixture was attained by smashing the prepared dried slurry and passing it by a screen (100-mesh). Finally, the green powder mixture was poured into a graphite die (diameter of 30 mm) to be densified at 1900 °C under 40 MPa for 10 min in a Nanozint 10i SPS facility (KPF Co., Iran). It is also worth mentioning that the inside of the graphite mold was lined with a soft graphite foil to prohibit any chemical reaction between the die and the mixture. However, such a line was removed via grinding after the SPS process.

The relative density of the SPSed composite was measured as a fraction of the bulk density estimated by the Archimedes principle to the theoretical density metered using the rule of mixture. The elemental assessment was performed using DXP-X10P energy-dispersive X-ray spectroscopy (EDS), whereas the phase analysis was carried out using Philips, PW1730 X-ray diffractometry (XRD). The former appliance was fitted with a Tescan Mira3 field emission scanning electron microscopy (Czech Republic) used in this study for microstructure assessment both on fracture and polished surfaces. In addition, a software called HSC (Outokumpu) was utilized for thermodynamic evaluations.

**Table 1.** The commercial raw materials used in this investigation as well as their relevant information.

| Powder | Particle size (μm) | Purity (%) | Manufacture |
|---|---|---|---|
| hBN | < 2 | > 98% | Xuzhou Hongwu Co., China |
| Ti | < 40 | > 98% | Sigma-Aldrich Co. |

## 3. Results and discussion

### *3.1. Sintering behavior and thermodynamic evaluation*

Based on the electron microscopy images and the XRD spectrums of as-purchased powders (not shown here), it can be noted that the morphology and particle size of each powder is in agreement with the datasheet presented by the manufacturer (Table 1). Additionally, the XRD spectrums imply that both starting materials were highly pure, and as a result, the amounts of possible impurities in these powders were such low that the XRD machine could not detect them. Nevertheless, as is well-known, the presence of oxide compounds on the surface of such powder particles is inevitable thanks to the high reactivity of both titanium and boron with the oxygen element available in the atmosphere. Accordingly, it can be assumed that Ti and BN powders are mainly covered by $TiO_2$ and $B_2O_3$ surface oxides, respectively, based on the literature.

Oxide impurities may have various roles in a specific sintering system. Briefly, oxide ingredients can either worsen or improve the sinterability of a ceramic-based composite. On the one hand, the presence of surface oxides on the adjacent particles, which are going to coalesce to each other, not only prohibits a powerful bonding between them, but also such contaminations may lead to grain coarsening during the sintering process. The latter phenomenon would be more problematic in the sintering routes with long soaking time, e.g., hot press and pressureless sintering. On the other hand, if the melting temperature of these oxide compounds would be lower than the maximum sintering temperature or they would be able to create a new low melting point ingredient together, a densification mechanism called liquid phase sintering can be activated over the process, boosting the sintering behavior of the composite. In any event, the assessment of the possible chemical interactions between the available phases, as well as recognition of the probable consolidation mechanisms over the sintering route, would be beneficial in finding a clear insight from the sintering behavior of a ceramic-based composite.

According to our calculation, the hBN-20 wt% Ti sample reached a relative density of 95.3%, which implies almost 5% remaining porosity in its microstructure. The XRD spectrum of this specimen is presented in Fig. 1. According to this pattern, the Ti content was totally consumed over the SPS process, and two in-situ phases, i.e., $TiB_2$ and

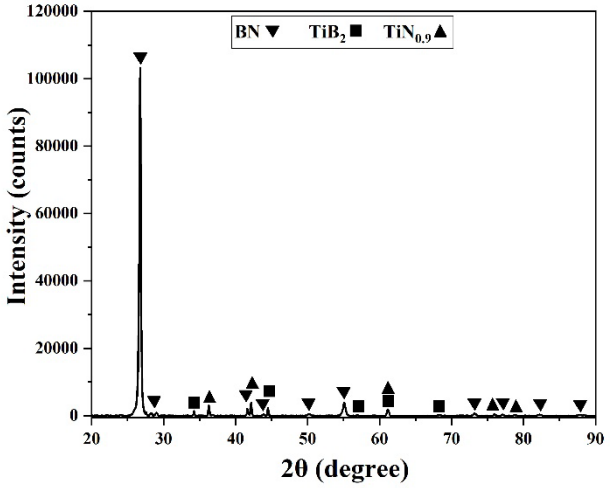


**Fig. 1.** The XRD spectrum of the hBN-20 wt% Ti.

$TiN_{0.9}$, were produced. In the following, the chemical reactions between the phases available in the hBN–Ti system will be evaluated.

First of all, as noted earlier, the hBN particles are inherently covered by the $B_2O_3$ oxide layer. This phase has a low melting point (between 450–510 °C), and as a result, forms a liquid phase (Eq. 1) at the initial steps of the SPS process. This phenomenon, as mentioned before, is called the liquid phase sintering mechanism, which is advantageous in enhancing the sinterability of the sample via particle rearrangement. In short, the existing particles may rearrange in a liquid bed, through which less free space remains amongst them. In addition, the fragmentation of large particles is another densification mechanism at low temperatures obtained as a result of the simultaneous applied pressure. Such a thing is also helpful in more reducing the free space

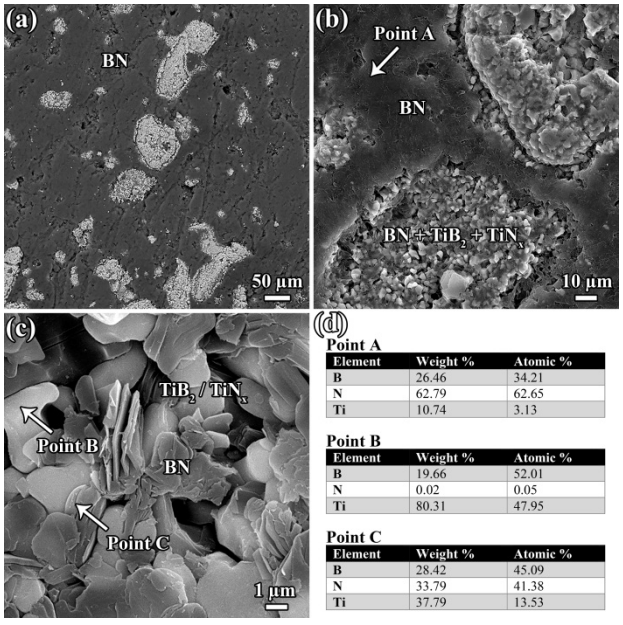


**Fig. 2.** The FESEM images from the polished surface of the hBN-20 wt% Ti specimen, together with the attributing EDS point analysis.

mentioned above. Although $B_2O_3$ has a controlling role in the sinterability of the hBN–Ti composite at low temperatures, it evaporates and leaves the system thanks to its low boiling point (1860 °C), as well as the high applied vacuum. This matter, along with the fact that $B_2O_3$ cannot chemically interact with other available phases in the system under the current sintering circumstances, reveals that such an oxide does not have any role in the sinterability of hBN–Ti at high temperatures.

Considering the $TiO_2$ oxide, the issue is utterly different. This oxide not only owns a higher melting point (1843 °C), but it also cannot evaporate and leave the system, due to its high boiling point (2972 °C). In other words, $TiO_2$ can generate a molten phase at the maximum sintering temperature, participating in filling the remaining porosity. This oxide finally solidifies as an amorphous compound in the microstructure. Similar to $B_2O_3$, $TiO_2$ cannot react with other existing ingredients and remain unreacted.

$$B_2O_3\ (s) = B_2O_3\ (l) \quad (1)$$

By contrast, BN and Ti have a strong reactivity to each other. In line with Eq. 2, Ti and BN ingredients can participate in a chemical reaction, generating in-situ $TiB_2$ and TiN phases. Such a reaction was evaluated using the HSC chemical package, and it was found that this reaction can easily advance at the current sintering system given its highly negative ΔG° at 1900 °C (almost -376 kJ). Olevsky et al. [35] also reported an equilibrium amongst the $TiB_2$, TiN, and BN phases in the ternary system of Ti–B–N. In view of the value calculated for the standard Gibbs free energy of Eq. 1, this fact that all Ti additive was consumed during the sintering process makes sense. However, the reason for identifying the TiN phase as a non-stoichiometric one in the XRD spectrum (Fig. 1) could be owing to the physical interaction between $TiB_2$ and TiN ingredients. Kitiwan et al. [39] scrutinized the binary system of TiN–$TiB_2$. Based on their study, when $TiB_2$ and TiN coexist under SPS conditions, they can lose boron and nitrogen, respectively. Such released atoms can diffuse into the other compound, forming a kind of solid solution. In other words, both $TiB_2$ and TiN phases may be non-stoichiometric with some point defects, namely substitutional or interstitial ones.

$$3Ti + 2BN = TiB_2 + 2TiN \quad (2)$$

### *3.2. Microstructural study*

Fig. 2a–c exhibits the FESEM micrographs from the polished section of the hBN-20 wt% Ti sample at different magnifications. Looking at Fig. 2a–b, some bright-colored regions are apparent, in which the added titanium reacted with the hBN matrix. According to the EDS point analysis from a point in the dark area (Fig. 2b), it is clear that the concentration of titanium is low in them, suggesting an almost pure hBN in such zones. By contrast, what happened within the bright colored areas is in agreement with the XRD analysis in Fig. 1. The high-magnification FESEM micrograph from such a zone (Fig. 2c) comprises some phases with different contrasts. On account of the EDS point analysis from the dark phase (not shown here), it was apparent that the dark ingredient in this image is associated with the remaining hBN. Additionally, the EDS result (Fig. 2d) related to the bright color compound (point B) revealed its consistency with the in-situ formed phase of $TiB_2$. Nevertheless, no distinct boundary was observable between these two phases, namely hBN and $TiB_2$. The EDS point

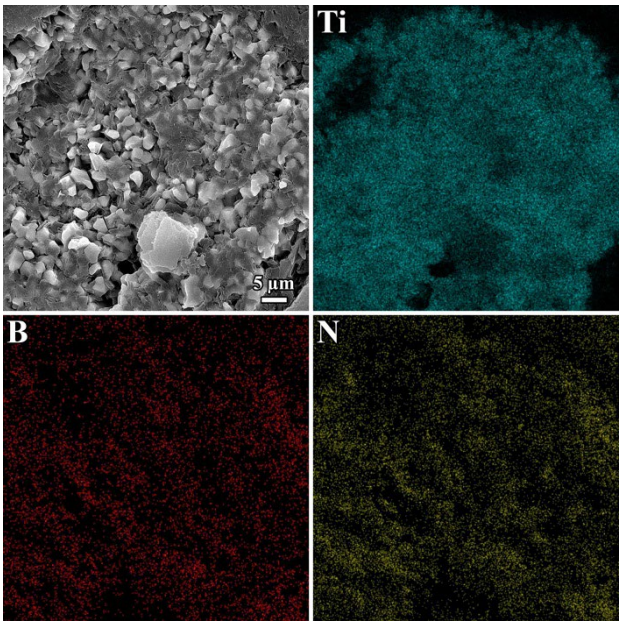


**Fig. 3.** The FESEM image from the polished surface of the hBN-20 wt% Ti sample, together with the attributing EDS map analysis.

analysis from point c as an intermediate zone indicated the high concentration of three elements of Ti, B, and N. This outcome is in harmony with our previous explanation about the possibility of diffusion of boron and nitrogen from in-situ phases of $TiB_2$ and TiN into each other. The EDS map analysis from an interaction zone (Fig. 3) can be beneficial in identifying the locations where various chemical compounds are available.

In terms of remaining porosity, it can be seen in both Fig. 2c and Fig. 3 that a considerable amount of porosity remained within the

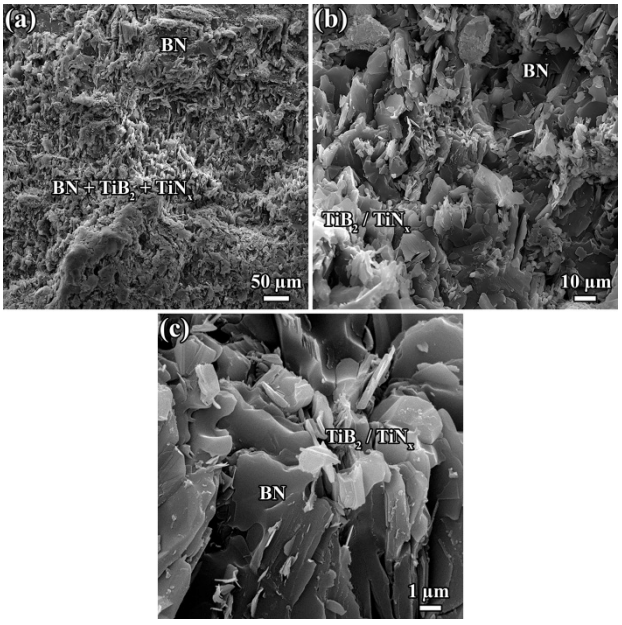


**Fig. 4.** The FESEM images from the fracture surface of the hBN-20 wt% Ti sample.

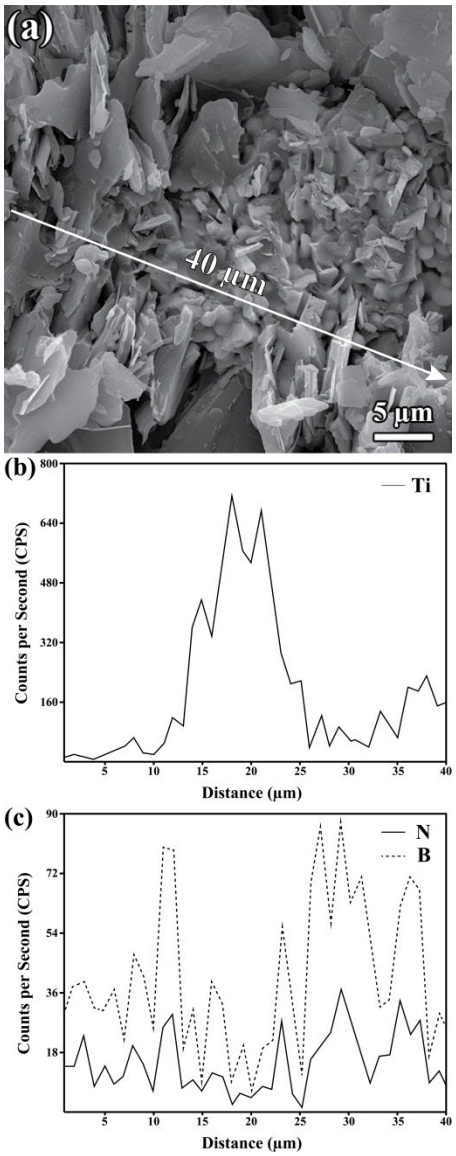


**Fig. 5.** The FESEM image from the fracture surface of the hBN-20 wt% Ti sample, together with the attributing EDS line results.

microstructure of the hBN-20 wt% Ti sample. Excluding the observable pores between the different available phases, indeed, some free space is available amongst the hBN platelets. Comparing the morphology of the starting hBN powder with that in Fig. 2c, it can be concluded that a new lamellar structure was formed over the sintering thanks to the nucleation and growth of the new hBN platelets. As such plates grow in one direction and there is no strong bonding between the grown platelets, some sub-micron porosity can be found in their intervals. Consequently, reaching a precise value of relative density for hBN-based materials would be challenging due to the difficulty of water penetration into the interval space.

Fig. 4 presents FESEM fractographs at different magnifications. Looking at these fractographs, the planar growth of new hBN platelets is clear. In addition, no distinct grains can be seen in these images, given the kind of recrystallization of the hBN particles. Nevertheless, some bright color phases are detectable in the fractographs, which are

associated with the in-situ synthesized $TiB_2$ and TiN ingredients. Although quite a few pores can be seen in these images, it should be taken into account that the majority of these free spaces are related to the pulled-out hBN plates over fracturing. Besides, Fig. 5 indicates a high-magnification fractography of the reaction zone in the hBN-20 wt% Ti specimen, together with the relevant EDS line results. As is apparent, each point possesses a unique chemical composition that could be due to the diffusion phenomenon, as explained earlier. It is also worth mentioning that the high reactivity of Ti with the hBN matrix prohibited the added Ti to act as a binder. In other words, as can be observed in the FESEM images, the incorporated Ti reacted with adjacent hBN matrix before it could be melted and fill the free spaces.

## 4. Conclusions

The hBN–Ti system was studied in this investigation by incorporating 20 wt% Ti as an additive into the hBN matrix. The sample was fabricated at 1900 °C via the SPS method, characterized by XRD, EDS, and FESEM. The composite reached a relative density of ~95%. The XRD spectrum revealed the total consumption of Ti during the SPS process, generating in-situ $TiB_2$ as well as non-stoichiometric $TiN_{0.9}$. The microscopical images indicated the nucleation and growth of the new hBN platelets from the initial fine particles. In addition, some boron and nitrogen atoms could leave the $TiB_2$ and TiN structures, respectively, diffusing into the other phases.

## CRediT authorship contribution statement

**Maryam Abdolahpour Salari:** Writing – review & editing, Project administration.
**Günay Merhan Muğlu:** Resources, Investigation.
**Mohsen Rezaei:** Visualization, Methodology.
**M. Saravana Kumar:** Conceptualization, Writing – review & editing.
**Harikrishnan Pulikkalparambil:** Resources, Supervision.
**Suchart Siengchin:** Writing – review & editing.

## Data availability

The data underlying this article will be shared on reasonable request to the corresponding author.

## Declaration of competing interest

The authors declare no competing interests.

## Funding and acknowledgment

We would like to express our gratitude to all the researchers who collaborated with the authors on this collaborative study involving Turkey, India, and Thailand.

## References

[1] T.B. Wang, C.C. Jin, J. Yang, C.F. Hu, T. Qiu, Physical and mechanical properties of hexagonal boron nitride ceramic fabricated by pressureless sintering without additive, Adv. Appl. Ceram. 114 (2015) 273–276. https://doi.org/10.1179/1743676114Y.0000000226.

[2] W.L. Du Frane, O. Cervantes, G.F. Ellsworth, J.D. Kuntz, Consolidation of cubic and hexagonal boron nitride composites, Diam. Relat. Mater. 62 (2016) 30–41. https://doi.org/10.1016/j.diamond.2015.12.003.

[3] X.J. Gao, D.M. Yan, J.W. Cao, C. Zhang, X.M. Mu, et al., The Study on the Property and the Microstructure of Pressureless Sintered h-BN Ceramics, Adv. Mater. Res. 1104 (2015) 9–14. https://doi.org/10.4028/www.scientific.net/amr.1104.9.

[4] X. Duan, D. Jia, Z. Wang, D. Cai, Z. Tian, et al., Influence of hot-press sintering parameters on microstructures and mechanical properties of h-BN ceramics, J. Alloys Compd. 684 (2016) 474–480. https://doi.org/10.1016/j.jallcom.2016.05.153.

[5] T. Hagio, H. Yoshida, Sintering and crystallization of ground hexagonal boron nitride powders, J. Mater. Sci. Lett. 13 (1994) 653–655. https://doi.org/10.1007/BF00271224.

[6] A. Lipp, K.A. Schwetz, K. Hunold, Hexagonal boron nitride: Fabrication, properties and applications, J. Eur. Ceram. Soc. 5 (1989) 3–9. https://doi.org/10.1016/0955-2219(89)90003-4.

[7] H. Yang, F. Gao, M. Dai, D. Jia, Y. Zhou, P. Hu, Recent advances in preparation, properties and device applications of twodimensional h-BN and its vertical heterostructures, J. Semicond. 38 (2017) 031004. https://doi.org/10.1088/1674-4926/38/3/031004.

[8] T. Hagio, K. Kobayashi, H. Yoshida, H. Yasunaga, H. Nishikawa, Sintering of the Mechanochemically Activated Powders of Hexagonal Boron Nitride, J. Am. Ceram. Soc. 72 (1989) 1482–1484. https://doi.org/10.1111/j.1151-2916.1989.tb07682.x.

[9] B. Ertug, Powder Preparation, Properties and Industrial Applications of Hexagonal Boron Nitride, Sinter. Appl. InTech. (2013). https://doi.org/10.5772/53325.

[10] C. Steinborn, M. Herrmann, U. Keitel, A. Schönecker, J. Räthel, et al., Correlation between microstructure and electrical resistivity of hexagonal boron nitride ceramics, J. Eur. Ceram. Soc. 33 (2013) 1225–1235. https://doi.org/10.1016/j.jeurceramsoc.2012.11.024.

[11] X. Gao, C. Zhang, P. Man, Y. Chang, B. Zhao, et al., Reaction mechanism and microstructure evolution of reaction sintered h-BN, J. Wuhan Univ. Technol. Mater. Sci. Ed. 32 (2017) 345–348. https://doi.org/10.1007/s11595-017-1601-2.

[12] H. Yang, H. Fang, H. Yu, Y. Chen, L. Wang, et al., Low temperature self-densification of high strength bulk hexagonal boron nitride, Nat. Commun. 10 (2019) 854. https://doi.org/10.1038/s41467-019-08580-9.

[13] X. Duan, D. Jia, Z. Wu, Z. Tian, Z. Yang, et al., Effect of sintering pressure on the texture of hot-press sintered hexagonal boron nitride composite ceramics, Scr. Mater. 68 (2013) 104–107. https://doi.org/10.1016/j.scriptamat.2012.09.012.

[14] J.X. Xue, J.X. Liu, B.H. Xie, G.J. Zhang, Pressure-induced preferential grain growth, texture development and anisotropic properties of hot pressed hexagonal boron nitride ceramics, Scr. Mater. 65 (2011) 966–969. https://doi.org/10.1016/j.scriptamat.2011.08.025.

[15] C. Xia, S.A. Delbari, Z. Ahmadi, M. Shahedi Asl, M. Ghassemi Kakroudi, et al., Electron microscopy study of ZrB2–SiC–AlN composites: Hot-pressing vs. pressureless sintering, Ceram. Int. 46 (2020) 29334–29338. https://doi.org/10.1016/j.ceramint.2020.08.054.

[16] V.H. Nguyen, S.A. Delbari, Z. Ahmadi, M. Shahedi Asl, M. Ghassemi Kakroudi, et al., Electron microscopy characterization of porous ZrB2–SiC–AlN composites prepared by pressureless sintering, Ceram. Int. 46 (2020) 25415–25423. https://doi.org/10.1016/j.ceramint.2020.07.011.

[17] M. Ghassemi Kakroudi, N. Pourmohammadie Vafa, M. Shahedi Asl, M. Shokouhimehr, Effects of SiC content on thermal shock behavior and elastic modulus of cordierite–mullite composites. Ceram. Int. 46 (2020) 23780–23784. https://doi.org/10.1016/j.ceramint.2020.06.153.

[18] M. Khoeini, A. Nemati, M. Zakeri, M. Shahedi Asl, Pressureless sintering of ZrB2 ceramics codoped with TiC and graphite, Int. J. Refract. Met. Hard Mater. 81 (2019) 189–195. https://doi.org/10.1016/j.ijrmhm.2019.02.026.

[19] N. Pourmohammadie Vafa, M. Ghassemi Kakroudi, M. Shahedi Asl, Role of h-BN content on microstructure and mechanical properties

of hot-pressed ZrB2–SiC composites, Ceram. Int. 46 (2020) 21533–21541. https://doi.org/10.1016/j.ceramint.2020.05.255.
[20] N. Pourmohammadie Vafa, M. Ghassemi Kakroudi, M. Shahedi Asl, Advantages and disadvantages of graphite addition on the characteristics of hot-pressed ZrB2–SiC composites. Ceram. Int. 46 (2020) 8561–8566. https://doi.org/10.1016/j.ceramint.2019.12.086.
[21] T.P. Nguyen, M. Ghassemi Kakroudi, M. Shahedi Asl, Z. Ahmadi, A. Sabahi Namini, et al., Influence of SiAlON addition on the microstructure development of hot-pressed ZrB2–SiC composites, Ceram. Int. 46 (2020) 19209–19216. https://doi.org/10.1016/j.ceramint.2020.04.258.
[22] S. Haji Amiri, M. Ghassemi Kakroudi, T. Rabizadeh, M. Shahedi Asl, Characterization of hot-pressed Ti3SiC2–SiC composites, Int. J. Refract. Met. Hard Mater. 90 (2020) 105232. https://doi.org/10.1016/j.ijrmhm.2020.105232.
[23] M. Ghassemi Kakroudi, M. Dehghanzadeh Alvari, M. Shahedi Asl, N. Pourmohammadie Vafa, T. Rabizadeh, Hot pressing and oxidation behavior of ZrB2–SiC–TaC composites, Ceram. Int. 46 (2020) 3725–3730. https://doi.org/10.1016/j.ceramint.2019.10.093.
[24] V.H. Nguyen, S.A. Delbari, M. Shahedi Asl, Q.V. Le, H.W. Jang, et al., A novel TiC-based composite co-strengthened with AlN particulates and graphene nano-platelets. Int. J. Refract. Met. Hard Mater. 92 (2020) 105331. https://doi.org/10.1016/j.ijrmhm.2020.105331.
[25] V.H. Nguyen, M. Shahedi Asl, Z. Hamidzadeh Mahaseni, M. Dashti Germi, S.A. Delbari, et al., Role of co-addition of BN and SiC on microstructure of TiB2-based composites densified by SPS method, Ceram. Int. 46 (2020) 25341–25350. https://doi.org/10.1016/j.ceramint.2020.07.001.
[26] B. Nayebi, N. Parvin, J. Aghazadeh Mohandesi, M. Shahedi Asl, Effect of Zr and C co-addition on the characteristics of ZrB2-based ceramics: Role of spark plasma sintering temperature, Ceram. Int. 46 (2020) 24975–24985. https://doi.org/10.1016/j.ceramint.2020.06.283.
[27] C. Xia, M. Shahedi Asl, A. Sabahi Namini, Z. Ahmadi, S.A. Delbari, et al. Enhanced fracture toughness of ZrB2–SiCw ceramics with graphene nano-platelets, Ceram. Int. 46 (2020) 24906–24915. https://doi.org/10.1016/j.ceramint.2020.06.275.
[28] V.H. Nguyen, Y. Pazhouhanfar, S.A. Delbari, S. Shaddel, A. Babapoor, et al., Beneficial role of carbon black on the properties of TiC ceramics, Ceram. Int. 46 (2020) 23544–23555. https://doi.org/10.1016/j.ceramint.2020.06.125.
[29] H. Istgaldi, B. Nayebi, Z. Ahmadi, P. Shahi, M. Shahedi Asl, Characterization of ZrB2–TiC composites reinforced with short carbon fibers, Ceram. Int. 46 (2020) 23155–23164. https://doi.org/10.1016/j.ceramint.2020.06.095.
[30] T. Kusunose, T. Sekino, Thermal conductivity of hot-pressed hexagonal boron nitride, Scr. Mater. 124 (2016) 138–141. https://doi.org/10.1016/j.scriptamat.2016.07.011.
[31] F.R. Zhai, M. Lu, K. Shan, Z.Z. Yi, Z.P. Xie, Spark plasma sintering and characterization of mixed h-bn powders with different grain sizes, Solid State Phenom. 281 (2018) 414–419. https://doi.org/10.4028/www.scientific.net/SSP.281.414.
[32] N. Ay, I. Tore, Pressureless Sintering of Hexagonal Boron Nitride Powders, Mater. Sci. Forum. 554 (2007) 207–212. https://doi.org/10.4028/www.scientific.net/msf.554.207.
[33] M. Shahedi Asl, S.A. Delbari, M. Azadbeh, A. Sabahi Namini, M. Mehrabian, et al., Nanoindentational and conventional mechanical properties of spark plasma sintered Ti–Mo alloys, J. Mater. Res. Technol. 9 (2020) 10647–10658. https://doi.org/10.1016/j.jmrt.2020.07.066.
[34] M. Hubacek, M. Ueki, Presuureless-sintered boron nitride with limithed content of boric oxide, J. Soc. Mater. Sci. 44 (1995) 209–212. https://doi.org/10.2472/jsms.44.507Appendix_209.
[35] F. Olevsky, P. Mogilevsky, E.Y. Gutmanas, I. Gotman, Synthesis of in situ TiB2/TiN ceramic matrix composites from dense BN-Ti and BN-Ti-Ni powder blends, Metall. Mater. Trans. A: Phys. Metall. Mater. Sci. 27 (1996) 2071–2079. https://doi.org/10.1007/BF02651860.
[36] T. Saito, F. Honda, Chemical contribution to friction behavior of sintered hexagonal boron nitride in water, Wear. 237 (2000) 253–260. https://doi.org/10.1016/S0043-1648(99)00346-4.
[37] Y .Cao, L. Du, C. Huang, W. Liu, W. Zhang, Wear behavior of sintered hexagonal boron nitride under atmosphere and water vapor ambiences, Appl. Surf. Sci. 257 (2011) 10195–10200. https://doi.org/10.1016/j.apsusc.2011.07.018.
[38] M. Kitiwan, A. Ito, T. Goto, Phase transformation and densification of hBN-TiN composites fabrication by spark plasma sintering, Key Eng. Mater. 508 (2012) 52–55. https://doi.org/10.4028/www.scientific.net/KEM.508.52.
[39] M. Kitiwan, A. Ito, T. Goto, B deficiency in TiB2 and B solid solution in TiN in TiN–TiB2 composites prepared by spark plasma sintering, J. Eur. Ceram. Soc. 32 (2012) 4021–4024. https://doi.org/10.1016/j.jeurceramsoc.2012.06.024.